CALPHAD: Computer Coupling of Phase Diagrams and Thermochemistry 51 (2015) 1–12

Contents lists available at ScienceDirect

CALPHAD: Computer Coupling of Phase Diagrams and Thermochemistry

journal homepage: www.elsevier.com/locate/calphad

Phase diagrams and thermochemical modeling of salt lake brine systems. I. LiCl+H_2O system

Dongdong Li [a,b], Dewen Zeng [a,c,*], Haijun Han [a], Lijiang Guo [a], Xia Yin [d], Yan Yao [a]

[a] Key Laboratory of Salt Lake Resources and Chemistry, Qinghai Institute of Salt Lakes, Chinese Academy of Sciences, Xining 810008, PR China
[b] University of Chinese Academy of Sciences, Beijing 100049, PR China
[c] College of Chemistry and Chemical Engineering, Central South University, Changsha 410083, PR China
[d] College of Chemistry and Chemical Engineering, Hunan University, Changsha 410082, PR China

ARTICLE INFO

Article history:
Received 26 January 2015
Received in revised form
13 May 2015
Accepted 14 May 2015

Keywords:
Phase diagram
Brine
Modeling
Pitzer–Simonson–Clegg model
LiCl

ABSTRACT

Salt lake brine chemical engineering involves the study of the solid–liquid equilibria of more than one hundred water–salt systems and approximately 70 solid salts over a wide temperature range. Prediction of the crystallization behavior of these complex systems as a function of temperature can only be achieved using a thermodynamic model. However, no systematic simulation studies have been reported for the complex salt lake brine systems, especially those systems containing the highly soluble salt LiCl. To complete this task, we plan to carry out a series of work. As the first part of the series of work, the Pitzer–Simonson–Clegg (PSC) model is selected to represent the thermodynamic properties of the LiCl+H_2O system in the temperature range of 190 K to nearly 400 K. In this model's framework, the temperature dependence of the thermodynamic functions (entropy, enthalpy and Gibbs energy) of the aqueous species and solid phases are determined using their heat capacities, which serves to keep their inner thermodynamics consistent and confers a strong extrapolation ability. The comprehensive thermodynamic properties, i.e., water activity, mean ionic activity coefficient, enthalpy of dilution and solution, heat capacity and solubility, are used to evaluate the model parameters. The proposed parameter regression strategy has proven successful for the LiCl+H_2O system. The present work forms a solid foundation for the simulation of thermochemical properties of other complicated salt lake brine systems.

1. Introduction

Salt lake brine and coexisting salt deposits are important inorganic mineral resources, from which a huge amount of valuable salts, i.e., potash fertilizer and lithium compounds, can be produced. Many salt lakes exist on Earth, and over thousands of them are located in China. Salt lake brines are complex multi-component electrolyte aqueous systems, which consist of many inorganic ions, e.g., Li^+, Na^+, K^+, Rb^+, Mg^{2+}, Ca^{2+}, Cl^-, SO_4^{2-}, CO_3^{2-}, HCO_3^-, NO_3^-, and borate. From these brines, dozens of solid salts can be crystallized under certain natural or artificial conditions. Depending on the chemical components of the brine, the salt lakes can be classified into chloride, chloride–sulfate, carbonate, and nitrate types. Because the brine compositions vary with regional characteristics, seasons, and solar evaporation stages, brine crystallization behaviors are very complex and differ from each other.

Usually, the humidity is very low in the regions where a salt lake is located. Salt evaporation pond process is one of the most economical tools to separate the salts from the brine. By adjusting the brine compositions in fractional crystallization processes, effective separation can be achieved. To obtain the desired salts, it is essential to know when and under what conditions (compositions and temperature) a specific type of salt will crystallize. Phase diagrams of the water–salt systems, if we have, can answer these questions. For decades, many authors have studied solid–liquid equilibria of simple binary, ternary and quaternary systems of salt lake brines at a scattered variety of temperatures. However, the exact crystallization sequence of salts and the appearance nodes of the salts cannot be determined from these scattered and limited experimental data alone. For a multi-component brine system, experimental determination of the phase diagram at a certain temperature is strenuous and time consuming work. Therefore, only the phase boundary, rather than a full characterization of the solid–liquid equilibria, is known for a given brine composition. Fortunately, phase diagram calculation approaches make it possible to reveal the phase equilibria behavior of a complex multi-

* Corresponding author at: Key Laboratory of Salt Lake Resources and Chemistry, Qinghai Institute of Salt Lakes, Chinese Academy of Sciences, Xining 810008, PR China.

http://dx.doi.org/10.1016/j.calphad.2015.05.001
0364-5916/

component system over the entire composition field using computer assisted simulation. Song and Yao [1] have extended the Pitzer's ion interaction model [2] to describe the excess thermodynamic properties of the simplified salt lake brine system of Li^+, Na^+, K^+, Mg^{2+}, Cl^-, SO_4^{2-}–H_2O at 25 °C. Applying the model with new model parameters, they have not only simulated the phase diagrams of this complicated system and its lower-order systems, but they have also predicted the salts crystallization sequence of any brine with a specific composition under isothermal evaporation conditions at 25 °C [3–5]. Kwok et al. [6] have also described the thermodynamic and phase equilibrium properties of the simplified salt lake brine system of Li^+, Na^+, K^+, Mg^{2+}, Cl^-, SO_4^{2-}–H_2O at 25 °C with an extended UNIQUAC equations [7]. Unfortunately, the validity of these models are limited to 25 °C, and cannot be used to predict the phase equilibria of this brine system at temperatures far away from 25 °C.

Most salt evaporation ponds are constructed near salt lakes, and the pond temperatures change with the local environment and seasons. The crystallization route of any brine with a specific composition can change with temperature. For example, halite usually precipitates from a chloride–sulfate type brine during evaporation processes in the summer, while mirabilite precipitates in the winter. Based on the fact that Li_2CO_3 solubility decreases with increasing temperature, a novel Li-extraction approach has been proposed to precipitate Li_2CO_3 from a carbonate-type brine at high temperatures [8]. In these cases, the influence of temperature on the crystallization route of brine can be significant. To understand the crystallization route of a brine at various temperatures, its solid–liquid phase diagram at various temperatures must be known. However, known thermodynamic models cannot represent the phase equilibria behavior of brine at various temperatures, especially for systems containing Li-salts. Some research groups [9–14] have extended the primitive Pitzer model to represent the solid–liquid phase diagram of oceanic salt systems, where Li-salts are absent, at multiple temperatures. For salt lake brine systems where Li-salts are present, the phase diagram simulation becomes challenging. Because Li-salts, such as LiCl, are very soluble, e.g., nearly 20 mol kg^{-1} at 25 °C and more than 30 mol kg^{-1} at 100 °C for LiCl, the primitive Pitzer model cannot successfully simulate the thermodynamic properties of the system [15]. A proper thermodynamic model should be chosen to simulate the salt lake brine containing Li-salts.

Based on the above considerations, we intend to develop a thermodynamically consistent model for the simulation of salt lake brine systems. This simulation will aid in the design of evaporation crystallization processes and optimization of salt lake brine. This series of work will begin with the simulation of simple binary and ternary systems at multiple temperatures, and it will gradually extend to more complex multi-component systems. In the first part of the series papers, the LiCl+H_2O system will be simulated, and the model selection and parameter determination methodology will be established.

2. Modeling methodology

2.1. Model selection

Pitzer's equations for most pure electrolytes are valid to a maximum of 6 mol kg^{-1} at 298.15 K with the parameters reported by Pitzer and co-workers [2]. Many publications [9–14] have shown that the Pitzer's model can be valid up to the solubility limits of most salts when proper parameters are introduced. Kim and Frederick [16] reported Pitzer ion interaction parameters for 304 single salts in aqueous solution valid up to nearly saturation at 298.15 K. Holmes and co-workers [17–19] have reported some temperature dependent Pitzer ion interaction parameters for pure salts determined from isopiestic results at elevated temperature. Many other temperature dependent ion interaction parameters have been summarized in a monograph by Pitzer [2]. Unfortunately, Pitzer's equations do not satisfactorily represent LiCl (aq) and $CaCl_2$(aq) systems at elevated temperature due to the very high concentrations of the solutions [15].

The assumption of a continuous solvent that is made in the primitive Pitzer model seems to be unreasonable for very concentrated aqueous solutions where the ion–water interactions are significantly strong. To describe the thermodynamic properties of very concentrated aqueous solutions, Pitzer and Simonson [20,21] proposed a mole fraction based ion interaction model. In this model, solvents are seen as particles instead of as a continuous medium, and a general Margules equation instead of virial expansion was introduced to describe the short range interactions of the particles. Clegg and Pitzer [22] and Clegg et al. [23] extended the Pitzer–Simonson equations to an indefinite number of components, including ions of different charge types. Unlike the Pitzer–Simonson equations, the Clegg–Pitzer equations used an asymmetric reference state. The final version of the mole fraction-based model equations proposed by Clegg et al. [23] is usually used and is called the Pitzer–Simonson–Clegg (PSC) model. The validity of these equations to very concentrated aqueous solutions has been widely proven [24–26]. Therefore, the PSC activity coefficient model is used to describe the non-ideality of the aqueous phase in this work and the following works of this series.

2.2. PSC-model description

The molar excess Gibbs energy (g^{ex}) equation and the derived equations for the activity coefficients (f_1, f_M^*andf_X^*), the apparent relative molal enthalpy ($^{\phi}L_m$), and the apparent molal heat capacity ($^{\phi}C_{p,m}$) of the PSC model for a pure electrolyte aqueous system $M_{\nu_M}X_{\nu_X}$ + H_2Owere derived by Clegg et al. [24] and are repeated here in Eqs. (1)–(7).

$$\begin{aligned} g^{ex}/RT = &-(4A_x/\rho)I_x \ln(1+\rho I_x) + x_M x_X B_{MX} g(\alpha I_x) \\ &+ x_M x_X B^1_{MX} g(\alpha_1 I_x) + 1/2(x_M Z_M + x_X Z_X)x_1(Z_M + Z_X) \\ &/(Z_M Z_X)W_{1,MX} + x_1 x_M x_X (Z_M + Z_X)^2/(Z_M Z_X)U_{1,MX} \\ &+ 4x_1^2 x_M x_X V_{1,MX} \end{aligned} \quad (1)$$

$$\begin{aligned} \ln f_1 = &\, 2A_x I_x^{3/2}/(1+\rho I_x^{1/2}) - x_M x_X B_{MX}\exp(-\alpha I_x^{1/2}) \\ &- x_M x_X B^1_{MX}\exp(-\alpha_1 I_x^{1/2}) + x_I^2 W_{1,MX} + x_I^2(x_I - x_1)U_{1,MX} \\ &+ 4x_1 x_M x_X (2 - 3x_1)V_{1,MX} \end{aligned} \quad (2)$$

$$\begin{aligned} \ln f_M^* = &-Z_M^2 A_x[(2/\rho)\ln(1+\rho I_x^{1/2}) \\ &+ I_x^{1/2}(1 - 2I_x/Z_M^2)/(1+\rho I_x^{1/2})] + x_X B_{MX} g(\alpha I_x^{1/2}) \\ &- x_M x_X B_{MX}[Z_M^2 g(\alpha I_x^{1/2})/(2I_x) \\ &+ (1 - Z_M^2/(2I_x))\exp(-\alpha I_x^{1/2})] + x_X B^1_{MX} g(\alpha I_x^{1/2}) \\ &- x_M x_X B^1_{MX}[Z_M^2 g(\alpha_1 I_x^{1/2})/(2I_x) \\ &+ (1 - Z_M^2/(2I_x))\exp(-\alpha_1 I_x^{1/2})] + x_1((Z_M + Z_X)/(2Z_X) - x_I) \\ &W_{1,MX} + x_1 x_I((Z_M + Z_X)/Z_X - 2x_I)U_{1,MX} + 4x_I^2 x_X(1 - 3x_M) \\ &V_{1,MX} - (1/2)[(Z_M + Z_X)/Z_X]W_{1,MX} \end{aligned} \quad (3)$$

$$\ln f_X^* = -Z_X^2 A_x[(2/\rho)\ln(1+\rho I_x^{1/2}) + I_x^{1/2}(1-2I_x/Z_X^2)/(1+\rho I_x^{1/2})] + x_M B_{MX} g(\alpha I_x^{1/2}) - x_M x_X B_{MX}[Z_M^2 g(\alpha I_x^{1/2})/(2I_x) + (1-Z_X^2/(2I_x))\exp(-\alpha I_x^{1/2})] + x_M B_{MX}^1 g(\alpha_1 I_x^{1/2}) - x_M x_X B_{MX}^1[Z_M^2 g(\alpha I_x^{1/2})/(2I_x) + (1-Z_X^2/(2I_x))\exp(-\alpha_1 I_x^{1/2})] + x_I((Z_M+Z_X)/(2Z_M) - x_I) W_{1,MX} + x_I x_I((Z_M+Z_X)/Z_M - 2x_I)U_{1,MX} + 4x_I^2 x_X(1-3x_X) V_{1,MX} - (1/2)[(Z_M+Z_X)/Z_M]W_{1,MX} \quad (4)$$

$$^{\varphi}L_m = \nu Z_M Z_X(A_{H,x}/2\rho)\ln(1+\rho I_x^{1/2}) - \nu x_I RT^2(Z_M Z_X/(Z_M+Z_X)^2)(B_{MX}^L g(\alpha I_x^{1/2}) + B_{MX}^{1,L} g(\alpha_1 I_x^{1/2})) + \nu x_I RT^2(W_{1,MX}^L - x_I U_{1,MX}^L - 4x_I^2(Z_M Z_X/(Z_M+Z_X)^2)V_{1,MX}^L) \quad (5)$$

$$^{\varphi}C_{p,m} = C_{p,m}^{\Theta} + \nu Z_M Z_X(A_{C,x}/2\rho)\ln(1+\rho I_x^{1/2}) - \nu x_I RT^2(Z_M Z_X/(Z_M+Z_X)^2)(B_{MX}^J g(\alpha I_x^{1/2}) + B_{MX}^{1,J} g(\alpha_1 I_x^{1/2})) + \nu x_I RT^2(W_{1,MX}^J - x_I U_{1,MX}^J - 4x_I^2(Z_M Z_X/(Z_M+Z_X)^2)V_{1,MX}^J) \quad (6)$$

where

$$g(x) = 2[1-(1+x)\exp(-x)]/x^2 \quad (7)$$

In the equations, $R=8.314$ J mol^{-1} K^{-1} is the gas constant, and T is the absolute temperature in Kelvin. A_x, $A_{H,x}$ and $A_{C,x}$ are the Debye–Hückel slopes for the mole fraction based ionic activity coefficient, enthalpy and heat capacity, respectively. The Bradley–Pitzer equation [27] for the dielectric constant and the Wagner–Pruss equation of state [28] for the density of pure liquid water are introduced to produce these Debye–Hückel slopes. ρ is a constant set to 13.0. I_x is the mole fraction based ionic strength ($I_x = (1/2)(Z_M^2 x_M + Z_X^2 x_X)$). The charge magnitudes of the ions M and X are Z_M and Z_X, respectively. The mole fraction of water is x_1, and x_I is the total mole fraction of the ions ($x_I = x_M + x_X$). ν ($\nu = \nu_M + \nu_X$) in Eqs. (5) and (6) is the number of moles of ions produced by the complete dissociation of one mole of the salt $M_{\nu_M}X_{\nu_X}$. $C_{p,m}^{\Theta}$ in Eq. (6) is the standard state heat capacity of the solute.

The temperature dependence of the PSC parameters ($P = B_{MX}$, B_{MX}^1, $W_{1,MX}$, $U_{1,MX}$ and $V_{1,MX}$) in the activity coefficient equations is defined in this work as

$$P(T) = a_0 + a_1 T + a_2 T\ln(T) + a_3 T^2 + a_4 T^3 + a_5/T \quad (8)$$

The temperature dependence of the parameters in Eqs. (5) and (6) for the respective enthalpy ($P^L = B_{MX}^L$, $B_{MX}^{1,L}$, $W_{1,MX}^L$, $U_{1,MX}^L$ and $V_{1,MX}^L$) and heat capacity ($P^J = B_{MX}^J$, $B_{MX}^{1,J}$, $W_{1,MX}^J$, $U_{1,MX}^J$ and $V_{1,MX}^J$) can be derived according to the definitions in Eqs. (9) and (10).

$$P^L(T) = \partial P(T)/\partial T \quad (9)$$

$$P^J(T) = \partial^2 P(T)/\partial T^2 + (2/T)\partial P(T)/\partial T \quad (10)$$

Generally, the experimental activity coefficient for the ions is a molality scale mean ionic activity coefficient ($\gamma_{\pm}$), and its relationship with the mole fraction based activity coefficients (f_M^* and f_X^*) is

$$\gamma_{\pm} = [(x_1 f_M^*)^{\nu_M}(x_1 f_X^*)^{\nu_X}]^{(1/\nu)} \quad (11)$$

Water activity (a_w) and the osmotic coefficient (ϕ) can be calculated from Eqs. (12) and (13).

$$a_w = x_1 f_1 \quad (12)$$

$$\phi = -(n_1/\nu n_2)\ln a_w \quad (13)$$

where, n_1 is the mole number of water, and n_2 is the mole number of the electrolyte.

2.3. Temperature dependence of the standard state thermodynamic properties

The standard Gibbs energy $G_i^{\Theta}(T)$ of any species i at temperature T can be calculated by following relationships:

$$G_i^{\Theta}(T) = H_i^{\Theta}(T) - S_i^{\Theta}(T)T = H_{i,298.15}^{\Theta} + \int_{298.15}^{T} C_{p,i}^{\Theta}(T)dT - (S_{i,298.15}^{\Theta} + \int_{298.15}^{T}\frac{C_{p,i}^{\Theta}(T)}{T}dT)T \quad (14)$$

So long the values of $H_{i,298.15}^{\Theta}$, $S_{i,298.15}^{\Theta}$ and $C_{p,i}^{\Theta}(T)$ are known, the value of $G_i^{\Theta}(T)$ can be calculated.

The temperature dependence of the standard isobaric heat capacity $C_{p,i}^{\Theta}$ for a species i is represented with Eq. (15) as recommended by the NIST Webbook [29].

$$C_{p,i}^{\Theta}(t) = A + Bt + Ct^2 + Dt^3 + E/t^2 \quad (15)$$

where, $t=(T/\text{K})/1000$, and T is the absolute temperature in Kelvin. A, B, C, D, and E are temperature coefficients.

Substituting Eq. (15) into Eq. (14), we have

$$H_i^{\Theta}(t) = At + Bt^2/2 + Ct^3/3 + Dt^4/4 - E/t + F \quad (16)$$

$$S_i^{\Theta}(t) = A\ln t + Bt + Ct^2/2 + Dt^3/3 - E/2t^2 + G \quad (17)$$

$$G_i^{\Theta}(t) = A(t - \ln t) - Bt^2/2 - Ct^3/6 - Dt^4/12 - E/2t + F - Gt \quad (18)$$

where

$$F = H_{i,298.15}^{\Theta} - (At_R + Bt_R^2/2 + Ct_R^3/3 + Dt_R^4/4 - E/t_R) \quad (19)$$

$$G = S_{i,298.15}^{\Theta} - (A\ln t_R + Bt_R + Ct_R^2/2 + Dt_R^3/3 - E/2t_R^2) \quad (20)$$

and $t_R = 0.29815$.

The temperature coefficients A, B, C, D, E, F, and G for the aqueous species $Li^+(aq)$ and $Cl^-(aq)$, liquid water, and ice are determined prior to regression of the PSC equation parameters.

The temperature coefficients A, B, C, D and E in Eq. (15) for the aqueous species $Li^+(aq)$ and $Cl^-(aq)$ are determined by fitting the individual isobaric heat capacity values calculated from the Helgeson–Kirkham–Flowers (HKF) equations of state (eos) [30,31] incorporated in the CHNOSZ software package [32] over the temperature range of 273.15 K to 523.15 K. $H_{i,298.15}^{\Theta}$ and $S_{i,298.15}^{\Theta}$ are calculated by the same software package, then from Eqs. (16) and (17) the coefficients F and G are determined.

The temperature coefficients in Eq. (15) for $H_2O_{(l)}$ listed in the NIST Webbook [29] are only valid in the temperature range from 298 K to 500 K, which is insufficient for the thermodynamic description of some electrolyte systems, such as $LiCl+H_2O$ where the solution temperature is as low as 194 K. Clegg and Brimblecombe [33] have discussed the problem of the heat capacity equation of supercooled water in detail. In the end, they adopted Hill's equation of state to derive a heat capacity equation for supercooled water that was valid to approximately 190 K, though the exploration of Hill's equation of state to subzero temperatures is inconsistent with the experimentally determined heat capacities of supercooled water [34,35]. We fit the experimental heat capacities of supercooled water using Eq. (15), and found that an accurate representation of the experimental data can only be obtained to approximately 230 K. Therefore, to obtain the temperature coefficients A, B, C, D, and E for $H_2O_{(l)}$ that are valid over a

Table 1
The experimental data used for parameter determination of the LiCl+H_2O system.

Experimental method	Data type	Fitted quantity	Temperature range/K	Composition range/mol kg^{-1}	Data points	σ_{est} [a]	σ_{fit} [b]	Ref.
Isopiestic	ϕ	ln a_w	318.15	0.5055–4.2057	19	0.003	0.0003	[42]
Isopiestic	ϕ	ln a_w	323.15	0.3322–2.0149	10	0.003	0.0002	[43]
Vapor pressure	ϕ	ln a_w	298.15–373.15	1.0208–18.585	54	0.003	0.0048	[44]
Tables	ϕ	ln a_w	298.15	0.001–19.219	43	0.003	0.0025	[45]
Isopiestic	R	ln a_w	382.96 - 443.92	0.6264–5.5658	118	0.003	0.0033	[46]
Vapor pressure	p	ln a_w	298.15	1.0–18.0	12	0.003	0.0051	[47]
Vapor pressure	p	ln a_w	398.15, 423.15	0.9934, 0.9946	2	0.003	0.0009	[48]
Isopiestic	a_w	ln a_w	298.15	0.3044–18.992	23	0.003	0.0073	[49]
Isopiestic	a_w	ln a_w	298.15	0.5181–19.848	21	0.003	0.0054	[50]
Tables	ϕ	ln a_w	298.15	0.1–20.0	51	0.003	0.0048	[51]
Isopiestic	ϕ	ln a_w	273.15	0.4819–9.1298	14	0.003	0.0040	[52]
Isopiestic	ϕ	ln a_w	323.15	0.8675–8.1272	14	0.003	0.0023	[53]
Isopiestic	R	ln a_w	428.65	7.4194–20.949	16	0.003	0.0101	[54]
Vapor pressure	p	ln a_w	291.15	0.725–15.59	14	0.003	0.0057	[55]
Vapor pressure	p	ln a_w	298.15	0–19.22	22	0.01	0.0223	[56]
Vapor pressure	p	ln a_w	303.15–373.15	3.496–18.675	72	0.005	0.0094	[57]
Vapor pressure	p	ln a_w	323.15–373.15	0.4479–3.202	18	0.005	0.0039	[58]
Isopiestic	ϕ	ln a_w	372.75	0.8–4.0	12	0.003	0.0016	[59]
Vapor pressure	p	ln a_w	303.15 – 343.15	3.01–18.456	40	0.005	0.0084	[60]
Freezing point	T_{fus}	ln a_w	197.45 – 262.35	2.5834–7.9476	8	0.003	0.0096	[61]
Freezing point	T_{fus}	ln a_w	205.15 – 268.05	1.294–7.5315	10	0.003	0.0079	[62]
Freezing point	ΔT_{fus}	ln a_w	267.52–273	0.04381–1.4216	16	0.003	0.0004	[63]
Freezing point	ΔT_{fus}	ln a_w	268.351–272.91	0.06–1.18	5	0.003	0.0014	[64]
Freezing point	ΔT_{fus}	ln a_w	251.61–273.1	0.0141–3.8946	22	0.003	0.0006	[65]
Saturated vapor pressure	p_{sat}	ln a_w	288.15–393.15	18.49–31.11	16	0.01	0.1146	[66]
Saturated vapor pressure	p_{sat}	ln a_w	333.6–413.25	23.39–31.68	15	0.01	0.0620	[67]
Saturated vapor pressure	p_{sat}	ln a_w	233.8–283.4	11.406–17.706	7	0.01	0.0528	[68]
e.m.f	$\gamma_\pm$	ln $\gamma_\pm$	273.15–308.15	0.05–5.0	19	0.003	0.0099	[69]
e.m.f	$\gamma_\pm$	ln $\gamma_\pm$	273.15–323,15	0.1–6.0	65	0.05	0.0524	[70]
Tables	$\gamma_\pm$	ln$\gamma_\pm$	298.15	0.001 – 19.219	43	0.005	0.0072	[45]
Tables	$\gamma_\pm$	ln $\gamma_\pm$	298.15	0.1–20.0	51	0.005	0.0110	[51]
Calorimetric	$\Delta_{dil}H_m$	$\Delta_{dil}H_m/RT$	373.15, 423.65	0.0155–16.508	37	0.008	0.0255	[71]
Calorimetric	$\Delta_{dil}H_m$	$\Delta_{dil}H_m/RT$	303.15	0.2416–1.1499	18	0.008	0.0147	[72]
Calorimetric	$\Delta_{dil}H_m$	$\Delta_{dil}H_m/RT$	298.15	0.1378–3.0	9	0.008	0.0142	[73]
calorimetric	$\Delta_{dil}H_m$	$\Delta_{dil}H_m/RT$	293.15	0.1388–2.2204	4	0.008	0.0197	[74]
Calorimetric	$\Delta_{dil}H_m$	$\Delta_{dil}H_m/RT$	298.15	0.25–6.75	9	0.008	0.0281	[75]
Calorimetric	$\Delta_{sol}H_m$	$^{\phi}L_m/RT$	298.15	0.1388–19.900	41	0.14	0.1358	[76]
Calorimetric	$^{\phi}C_{p,m}$	$^{\phi}C_{p,m}/R$	298.15	0.0455–0.1	3	0.6	0.2417	[77]
Calorimetric	$^{\phi}C_{p,m}$	$^{\phi}C_{p,m}/R$	298.15	0.1–0.96	8	0.06	0.2728	[77]
Calorimetric	$^{\phi}C_{p,m}$	$^{\phi}C_{p,m}/R$	303.15–403.15	0.497–1.755	33	0.06	0.2542	[78]
Calorimetric	$^{\phi}C_{p,m}$	$^{\phi}C_{p,m}/R$	298.15	0.04–2.4614	17	1.55	0.7583	[79]
Calorimetric	c_p	$^{\phi}C_{p,m}/R$	308.15–343.15	4.1630–19.316	56	0.06	0.1102	[80]
Calorimetric	c_p	$^{\phi}C_{p,m}/R$	299.65	0.00–19.8779	36	0.12	0.3120	[76]
Calorimetric	c_p	$^{\phi}C_{p,m}/R$	293	2.2204	4	0.06	0.1497	[74]
Thermal analysis	(T, m_s)	ln K	199.25–249.45	8.3101–13.1835	8	0.02	0.0595	[61]
Visual polythermal	(T, m_s)	ln K	194.65–291.4	8.2455–19.1924	28	0.02	0.03	[62]
Visual polythermal	(T, m_s)	ln K	207.75–333.15	9.7057–23.3651	23	0.02	0.0316	[81]
Isothermal	(T, m_s)	ln K	273.15–372.65	16.064–29.83	14	0.02	0.0358	[82]
Isothermal	(T, m_s)	ln K	273.15, 290.65	16.064–18.9993	2	0.02	0.0219	[83]
Isothermal	(T, m_s)	ln K	273.15, 373.15	16.325, 29.78	2	0.02	0.0368	[84]
Isothermal	(T, m_s)	ln K	273.15, 353.15	16.305, 26.294	4	0.02	0.0253	[85]
Isothermal	(T, m_s)	ln K	273.15, 323.15	16.211, 22.056	2	0.02	0.0133	[86]
Isothermal	(T, m_s)	ln K	283.15, 323.15	17.536, 21.986	2	0.02	0.0182	[87]
Isothermal	(T, m_s)	ln K	274.2–413.45	16.325–32.981	14	0.02	0.0138	[67]
Isothermal	(T, m_s)	ln K	273.15–361.15	16.292–28.3023	21	0.02	0.0192	[88]
Isothermal	(T, m_s)	ln K	344.65–413.65	25.160–33.199	15	0.02	0.0113	[89]
Visual polythermal	(T, m_s)	ln K	277.45–398.12	16.8596–32.06	18	0.02	0.0164	[90]
Isothermal	(T, m_s)	ln K	291.15	19.5523	1	0.02	0.0331	[55]
Isothermal	(T, m_s)	ln K	298.15	19.9585	1	0.02	0.0144	[51]
Isothermal	(T, m_s)	ln K	298.15	19.2234	1	0.02	0.1313	[56]

[a] Estimated standard deviation as respect to the fitted quantity.
[b] Standard deviation of the fitting as respect to the fitted quantity.

wide temperature from 190 K to 523 K, we fit them to the heat capacities of water calculated from Hill's equation of state at temperatures below zero and the NIST Webbook equation at temperatures above zero. From the standard enthalpy and entropy of $H_2O_{(l)}$ at 298.15 K listed in the NIST Webbook, the coefficients F and G for $H_2O_{(l)}$ are determined with Eqs. (19) and (20).

Feistel and Wagner [36] listed individual evaluated heat capacities of $H_2O_{(cr,I)}$ from 0 K to 273 K, from which the temperature coefficients A, B, C, D, and E for $H_2O_{(cr,I)}$ are determined by fitting over the temperature range from 180 K to 273 K. Starting from the enthalpy (-292.744 kJ mol^{-1}) and entropy (44.776 J mol^{-1} K^{-1}) of ice at 298.15 K reported by Kobylin et al. [37], the standard Gibbs energy of $H_2O_{(cr,I)}$ as a function of temperature in the form of Eq. (18) is determined.

To simulate the solid–liquid equilibria (SLE), the standard Gibbs free energy $G_i^{\theta}(T)$ for a solid phase $M_{\nu_M}X_{\nu_X}{\cdot}nH_2O_{(s)}$ as function of temperature, i.e., Eq. (18), is necessary. These coefficients can be

Table 2
Gibbs free energy functions of aqueous and solid species in the LiCl+H_2O system at standard state.

Species	$G_f^{\Theta}(t) = A(t - \ln t) - Bt^2/2 - Ct^3/6 - Dt^4/12 - E/2t + F - Gt$[a]							
	A	*B*	*C*	*D*	*E*	*F*	*G*	*T*/K
$Li^+_{(aq)}$[b]	4908.41	−26,562.4	54573.6	−40,213.6	−63.4622	−1176.824	11,443.528	273–523
$Cl^-_{(aq)}$[b]	29,421.3	−157,725	316,626	−227,316	−412.404	−5660.068	68,302.467	273–523
$H_2O_{(l)}$[c]	−90.0669	748.166	−1377.94	1055.31	3.26118	−271.203	−191.886	180–523
$H_2O_{(cr,I)}$[d]	13.44	20.2535	371.643	−418.377	−0.0301987	−300.209	42.01	100–273
$LiCl_{(cr)}$[e]	43.7437	20.3706	0.3064	−0.0942	−0.1604	−423.3378	106.7998	368–403
$LiCl \cdot H_2O_{(cr)}$[f]	−429.3131	1746.9163	0	0	0	−662.5562	−940.5144	291–371
$LiCl \cdot 2H_2O_{(cr)}$[f]	112.3047	76.2211	0	0	0	−1050.1934	251.3980	248–292
$LiCl \cdot 3H_2O_{(cr)}$[f]	−1447.8245	5454.8197	0	0	0	−1126.6395	−3220.1464	205–253
$LiCl \cdot 5H_2O_{(cr)}$[f]	−3647.1742	13,123.2743	0	0	0	−1417.0329	−8150.9733	194–208

[a] $t=(T/K)/1000$.
[b] The parameters *A*, *B*, *C*, *D*, and *E* are determined by fitting the heat capacity values calculated from the HKF eos [30, 31] temperature from 273.15 K to 523.15 K, and further the parameters *F* and *G* are determined from Eqs. (19) and (20) with the calculated standard enthalpy of formation and standard entropy from the same eos at 298.15 K.
[c] See text.
[d] The parameters *A*, *B*, *C*, *D*, and *E* are determined from the evaluated heat capacity of H_2O(cr, I) [36], and the standard enthalpy of formation and standard entropy of ice at 298.15 K are taken from [37].
[e] The parameters *A*, *B*, *C*, *D*, and *E* are taken from the NIST webbook [29], and the parameters *F* and *G* are determined in this work.
[f] All parameters are determined in this work.

Table 3
The assessed PSC equation parameters for LiCl(aq) in this work according to Eq. (8).[a]

Parameter	$P(T) = a_0 + a_1T + a_2T\ln(T) + a_3T^2 + a_4T^3 + a_5/T$					
	a_0	a_1	a_2	a_3	a_4	a_5
B_{MX}	1.3010382052E+05	−3.1705782693E+03	5.3668013223E+02	−9.5789670500E−01	3.0982145524E−04	−5.8444748172E+06
B^1_{MX}	−1.2387122226E+04	6.3919531162E+01	−1.4788013388E−01	−1.4622455132E−01	1.2411839690E−04	1.0684222082E+06
$W_{1,MX}$	−1.3864671327E+04	3.3123688967E+02	−5.5662564035E+01	9.2621743326E−02	−2.5628544062E−05	6.3728226406E+05
$U_{1,MX}$	−2.2118502055E+04	5.6608505408E+02	−9.6801383941E+01	1.8397236076E−01	−6.3850511009E−05	9.3580509545E+05
$V_{1,MX}$	7.6423337014E+03	−1.7462518431E+02	2.8910893675E+01	−4.1523732843E−02	7.3586558412E−06	−3.6887115877E+05

[a] $\alpha=13.0$, $\alpha_1=2.0$

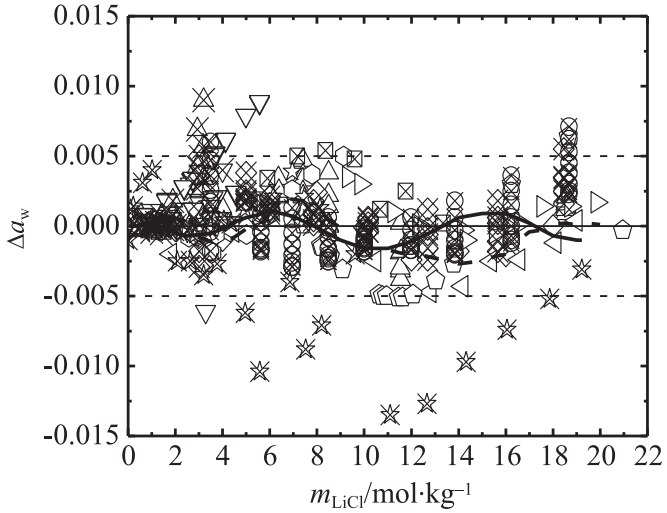

Fig. 1. Differences $\Delta a_w = a_w(\text{expt}) - a_w(\text{calc})$ of the experimental water activities from those calculated in this work for unsaturated solution. □: 318.15 K [42], ○: 323.15 K [43], △: 298.15 K to 373.15 K [44], ▽: 382.96 K to 473.61 K [46], ◇: 298.15 K [47], ◁: 298.15 K [49], ▷: 298.15 K [50], ⬡: 273.15 K [52], ☆: 323.15 K [53], ⬠: 428.65 K [54], ◁: 291.15 K [55], ✳: 298.15 K [56], ⊠: 303.15 K to 373.15 K [57], ⊠: 323.15 K to 373.15 K [58], ✳: 372.75 K [59], ⊠: 303.15 K to 343.15 K [60], thick solid line: 298.15 K table values [45], thick dash line: 298.15 K table values [51].

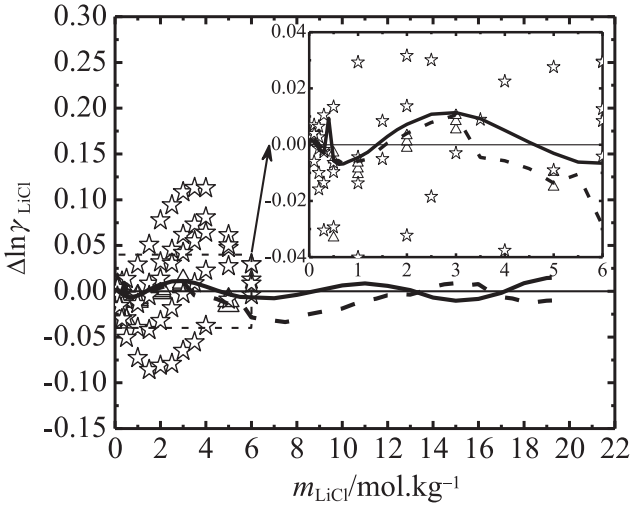

Fig. 2. Difference $\Delta \ln \gamma_{LiCl} = \ln \gamma_{LiCl}(\text{expt}) - \ln \gamma_{LiCl}(\text{calc})$ of the experimental mean ionic activity coefficients from those calculated with this model. △: [69], ☆: [70], thick solid line: 298.15 K [45], thick dash line: 298.15 K [51].

obtained by fitting the SLE data of the dissolution reaction:

$$M_{\nu_M}X_{\nu_X}\cdot nH_2O_{(s)} = \nu_M M^{\nu_{X+}}_{(aq)} + \nu_X X^{\nu_{M-}}_{(aq)} + nH_2O_{(l)} \quad (21)$$

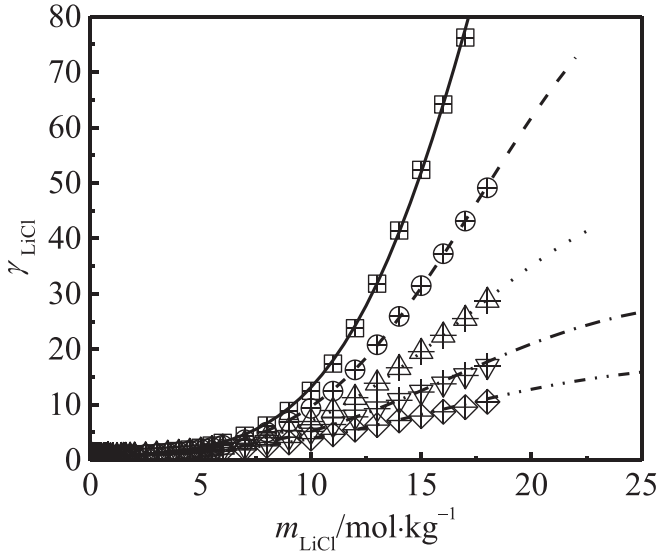

Fig. 3. Mean ionic activity coefficients of LiCl(aq) at various temperatures. All symbols are literature data [44]: ⊞, 273.15 K; ⊕, 298.15 K; ⧋, 323.15 K; ⧩, 348.15 K, ⊕, 373.15 K. All lines are model values in this work.

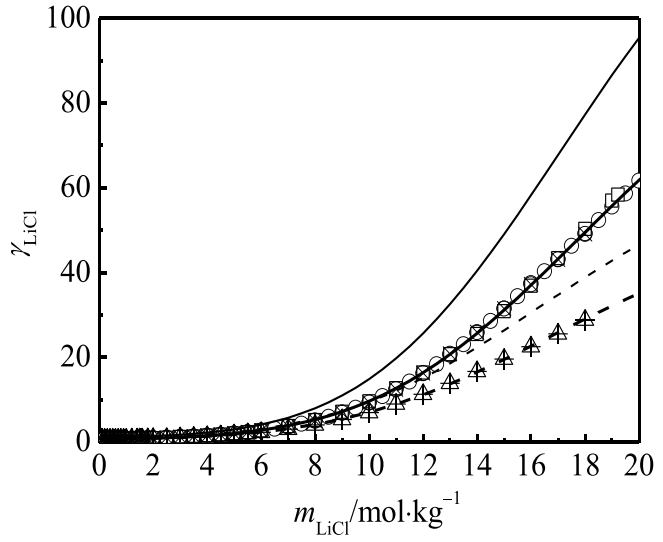

Fig. 4. Mean ionic activity coefficients of LiCl(aq) at various temperatures. ⊕: 298.15 K [44], ⧋: 323.15 K [44], □: 298.15 K [45], ◯: 298.15 K [51], thick solid line: model values at 298.15 K in this work, thick dash line: model values at 323.15 K in this work, thin solid line: calculated with the model parameters in Ref. [92] at 298.15 K, thin dash line: calculated with the model parameters in Ref. [92] at 323.15 K.

at various temperatures with the following thermodynamic relationships

$$G^{\Theta}_{m,M_{v_M}X_{v_X}\cdot nH_2O_{(s)}} = v_M G^{\Theta}_{m,M^{v_{X+}}_{(aq)}} + v_X G^{\Theta}_{m,X^{v_{M-}}_{(aq)}} + nG^{\Theta}_{m,H_2O_{(l)}} + RT\ln K \quad (22)$$

where $K = a_M^{v_M} a_X^{v_X} a_{H_2O}^{n}$, $G^{\Theta}_{m,M_{v_M}X_{v_X}\cdot nH_2O_{(s)}}$, $G^{\Theta}_{m,M^{v_{X+}}_{(aq)}}$, $G^{\Theta}_{m,X^{v_{M-}}_{(aq)}}$, and $G^{\Theta}_{m,H_2O_{(l)}}$ are the standard molar Gibbs free energies of $M_{v_M}X_{v_X}\cdot nH_2O_{(s)}$, $M^{v_{X+}}_{(aq)}$, $X^{v_{M-}}_{(aq)}$, and $H_2O_{(l)}$, respectively. a_i is the activity of substance i at saturation.

To eliminate the arbitrary nature of the parameters in Eq. (18) for a certain solid and to make the parameters more physically meaningful, the temperature coefficients A, B, C, D, and E are fixed in advance according to the heat capacities in the form of Eq. (15). In most cases, the heat capacities of anhydrous salt solids are available. In the cases where the heat capacities of hydrated salts

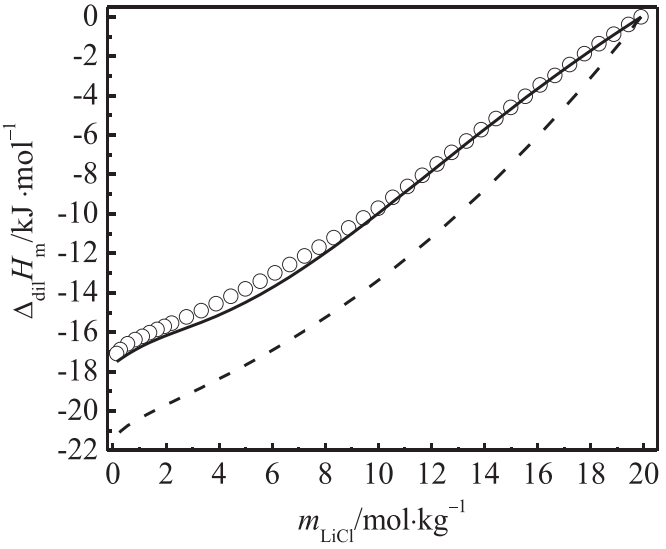

Fig. 5. Plot of enthalpies of dilution against molality at 298.15 K for LiCl(aq). The initial molality is $m_1 = 19.001$ mol kg^{-1}. The enthalpies of dilution are plotted as a function of the final molality m_2. ◯: [76], and solid line: model values in this work, dash line: model values in the literature [93].

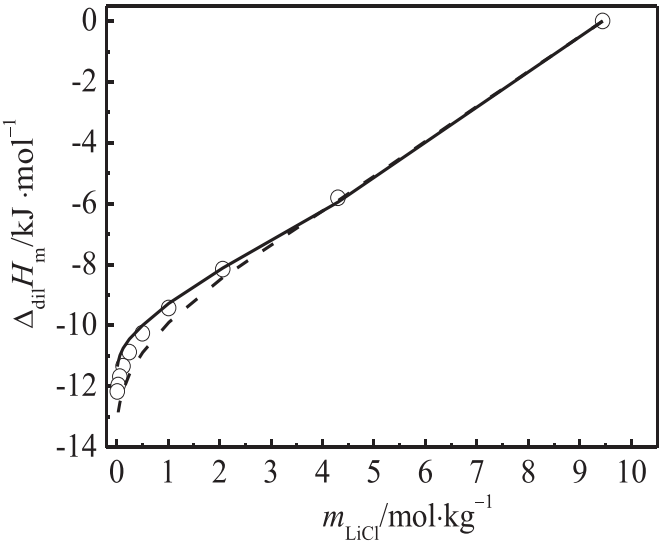

Fig. 6. Plot of enthalpies of dilution against molality at 373.15 K for LiCl(aq). The initial molality is $m_1 = 9.443$ mol kg^{-1}. The enthalpies of dilution are plotted as a function of the final molality m_2. ◯: [71], solid line: this model values, dash line: model values in the literature [93].

are unavailable, the following two approximation evaluation approaches are used:

(1) An additivity rule is applied to estimate the heat capacity of a hydrated salt as a function of temperature, as expressed by Eq. (23).

$$C^{\Theta}_{p,MX\cdot nH_2O_{(s)}}(t) = C^{\Theta}_{p,MX_{(s)}}(t) + nC^{\Theta}_{p,H_2O} \quad (23)$$

where $C^{\Theta}_{p,MX\cdot nH_2O_{(s)}}(t)$ and $C^{\Theta}_{p,MX_{(s)}}(t)$ are the heat capacity of the hydrated and anhydrous salt at temperature t, respectively, and $C^{\Theta}_{p,H_2O_{(l)}}$ is the group contribution of one crystal water molecular to the heat capacity of the hydrated salt independent of temperature and set to 43.5 J K^{-1} mol^{-1} as recommended by Archer [38].

(2) An alternative approach is to express the heat capacity of a hydrated salt solid using a simplified form Eq. (24):

$$C^{\Theta}_{p,MX\cdot nH_2O_{(s)}}(t) = A + Bt \quad (24)$$

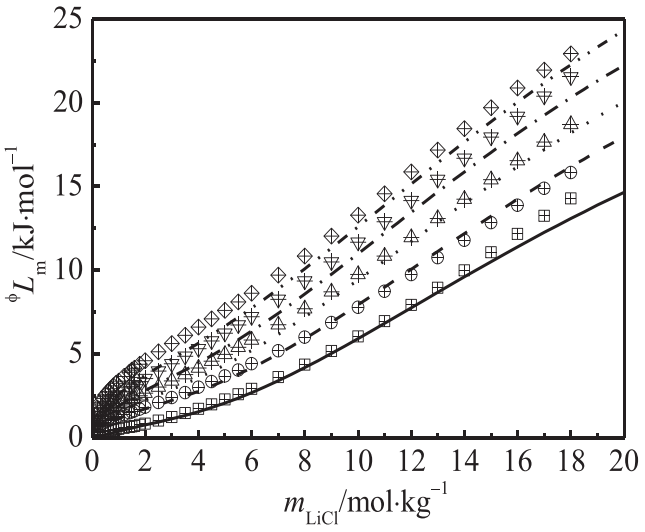

Fig. 7. Apparent relative molal enthalpies of LiCl(aq) at various temperatures. Symbols: literature values [44], ⊞: 273.15 K, ⊕: 298.15 K, ⧋: 323.15 K, ⧩: 348.15 K, ⊜: 373.15 K. Lines: this model values, solid line: 273.15 K, dash line: 298.15 K, dot line: 323.15 K, dash dot line: 348.15 K, dash dot dot line: 373.15 K.

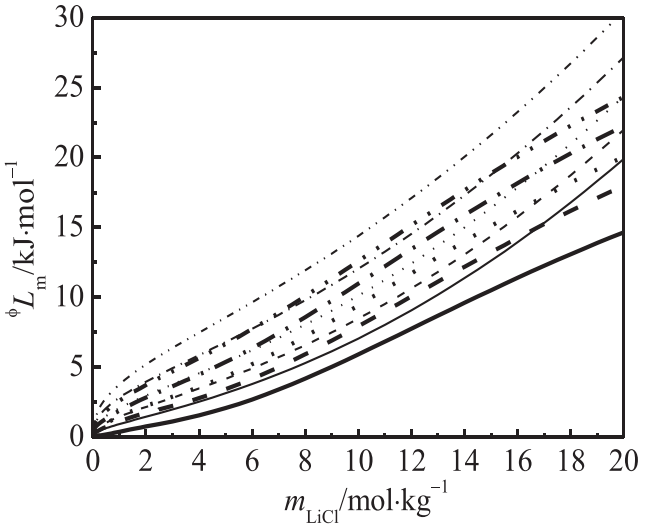

Fig. 8. Comparisons of the apparent relative molal enthalpies of LiCl(aq). Thick lines, this work; thin lines, Holmes and Mesmer [93]; solid line: 273.15 K, dash line: 298.15 K, dot line: 323.15 K, dash dot line: 348.15 K, dash dot dot line: 373.15 K.

When the heat capacity at 298.15 K is known, Eq. (24) can be simplified as

$$C^{\Theta}_{p,MX\cdot nH_2O_{(s)}}(t) = C^{\Theta}_{p,MX\cdot nH_2O_{(s)}}(0.29815) + (t - 0.29815)B \tag{25}$$

In this case, the parameter $C^{\Theta}_{p,MX\cdot nH_2O_{(s)}}(0.29815)$ is evaluated by Eq. (23).

The remaining coefficients B, F and G for all salts (anhydrous and hydrated), along with the PSC model parameters, are regressed by fitting the experimental activity and thermal property data for the aqueous phases, as well as the SLE data.

3. Parameter regression method

Multiple properties of an electrolyte system, i.e., water activity (a_w), mean ionic activity coefficient ($\gamma_{\pm}$), enthalpy of dilution ($\Delta_{dil}H_m$), apparent relative molal enthalpy ($^{\phi}L_m$), apparent molal heat capacity ($^{\phi}C_{p,m}$) and solid–liquid equilibria data (T, m_s), are

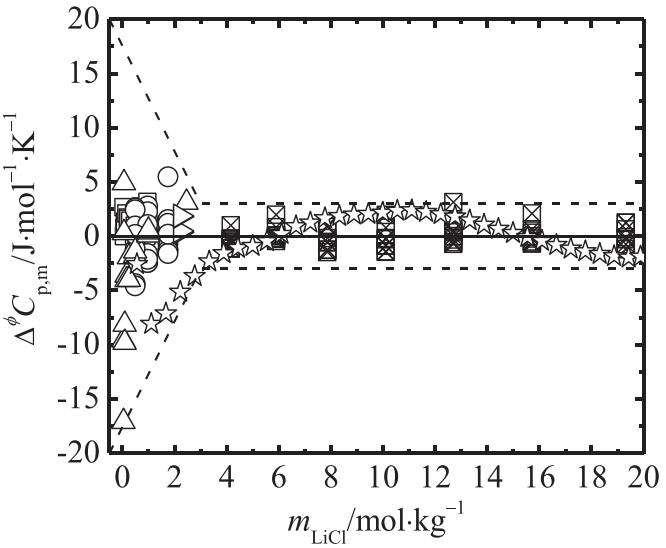

Fig. 9. Difference $\Delta^{\phi}C_{p,m}={}^{\phi}C_{p,m}(\text{expt})-{}^{\phi}C_{p,m}(\text{calc})$ of the experimental apparent molal heat capacity of LiCl(aq) from those calculated with this model. ▷: [74], ☆: [76], □: [77], ○: [78], △: [79], ◁: [80]. Dash lines: evaluated measurement errors of apparent molal heat capacity.

used simultaneously to regress the model parameters using a weighted least square method.

The objective function (OF) of a weighted least square is

$$OF = \sum_{i=1}^{n} w_i(P_i^c - P_i^e)^2 \tag{26}$$

where n is the number of properties (expressed as P_i) to be reproduced, P_i^c, P_i^e and w_i are the calculated and experimental values of property i and the weight factor of property i, respectively. w_i values are calculated from the standard deviation σ_i of property i from Eq. (27)

$$w_i = \frac{1}{\sigma_i^2} \tag{27}$$

where, the standard deviation σ_i of property i is estimated with the following steps: (1) To get a initial estimate on σ_i of property i (for each set of data the σ_i is the same), each set of data listed in Table 1 are fitted with the thermodynamic model separately. (2) With these estimated standard deviations of each set of data, all the data are fitted in one simultaneous, and then the standard deviations of overall fitting are calculated and compared with the initial estimates. (3) Adjust the initial estimates of the standard deviations to meet the overall fitting, and then go to (2) until all the new generated standard deviations are agreed with the values of the overall fitting generally.

The property terms include ln a_w, ln$\gamma_{\pm}$, $\Delta_{dil}H_m/RT$, $^{\phi}L_m/RT$, $^{\phi}C_{p,m}/R$, and ln K and are approximately in the same order of magnitude. A parameter regression program named PSCBREG was written for this purpose, where the standard weighted linear least squares algorithm implemented in the GNU scientific library [39] is called for the optimization.

For the experimental data given in a form other than a_w, $\gamma_{\pm}$, $\Delta_{dil}H_m$, $^{\phi}L_m$, or $^{\phi}C_{p,m}$, necessary conversions have been made to adapt to the parameter regression program.

Experimental osmotic coefficients given in isopiestic ratios referred to NaCl(aq) are converted to water activity a_w as a function of NaCl concentration recommended by Pitzer et al. [40].

Vapor pressure data are converted to water activity a_w with the following equation:

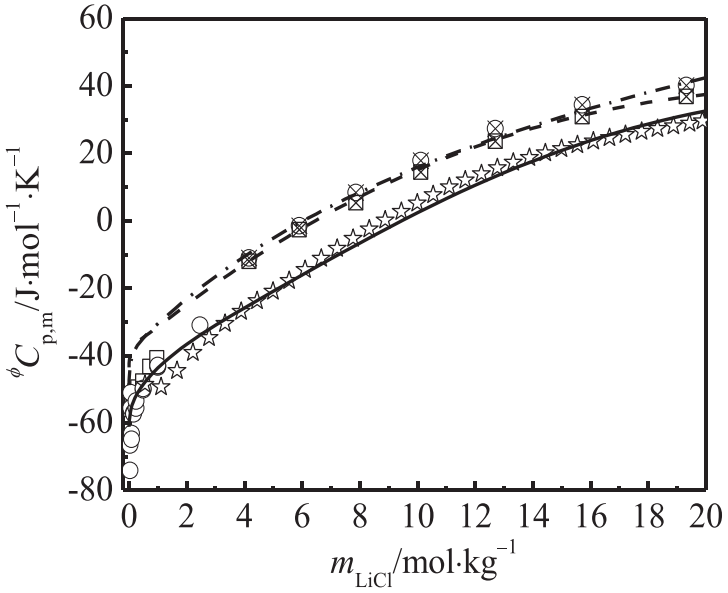

Fig. 10. Apparent molal heat capacities of LiCl(aq) at about 299.65 K, 323.15 K and 343.15 K. ☆: 299.65 K [76], ◯: 298.15 K [77], □: 298.15 K [79], ◁: 323.15 K [80], ⊠: 343.15 K [80]. Lines: this model values, solid line: 299.65 K, dash line: 323.15 K, dash dot line: 343.15 K.

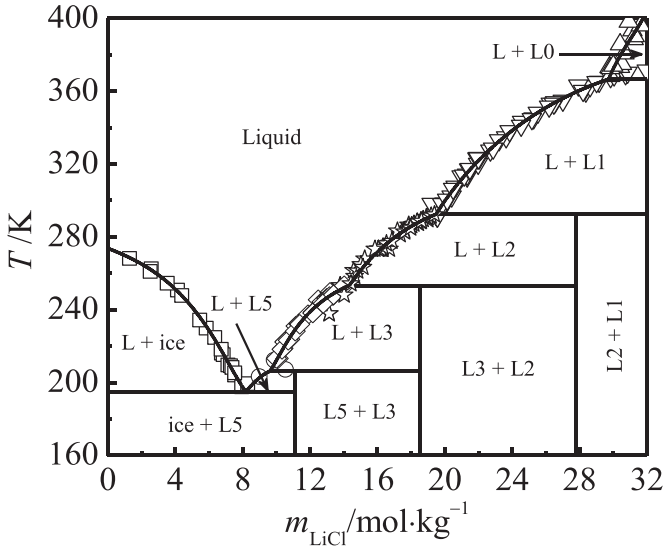

Fig. 11. Phase diagram of LiCl+H_2O system temperature from 160 K to 400 K. L: Liquid, L0: LiCl(cr), L1: LiCl · H_2O(cr), L2: LiCl · $2H_2O$(cr), L3: LiCl · $3H_2O$(cr), L5: LiCl · $5H_2O$(cr). □: ice [61,62], ◯: L5 [61], ◇: L3 [61,62,81], ☆: L2 [61,62,67,81–83, 85–88,90], ▽: L1 [51,55,56,82,85–90], △: L0 [67,82,84,89,90].

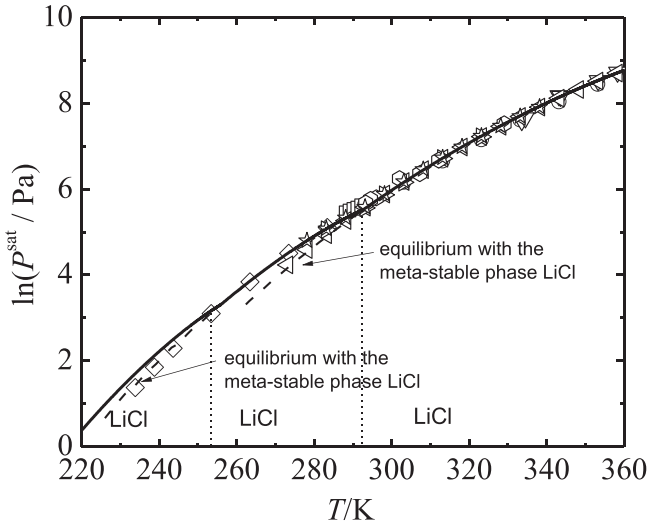

Fig. 12. Vapor pressures of the LiCl(aq) solution saturated with LiCl · H_2O(cr), LiCl · $2H_2O$(cr) and LiCl · $3H_2O$(cr). □: LiCl · $2H_2O$(cr) [66], ◯: LiCl · H_2O(cr) [66], ▽: LiCl · H_2O(cr) [67], ⬡: solid phase unknown [94], ☆: solid phase unknown [95], ▷: solid phase unknown [96], ◁: solid phase unknown [97], ◇: solid phase unknown [68], solid line: this model values (stable equilibria), dash line: this model values (metastable equilibria).

$$\ln a_w = \ln\left(\frac{p}{p_0}\right) + \frac{B_T(p - p_0)}{RT} \tag{28}$$

where B_T is the second virial coefficient taken from Ref. [41], and p_0 is the vapor pressure of pure water taken from Ref. [28].

Data of freezing point or freezing point depression are converted to water activity by the following relation:

$$G^{\Theta}_{m,H_2O_{(s)}} = G^{\Theta}_{m,H_2O_{(l)}} + RT \ln a_w \tag{29}$$

where $G^{\Theta}_{m,H_2O_{(s)}}$ and $G^{\Theta}_{m,H_2O_{(l)}}$ are already known.

Experimental data of the enthalpy of solution are converted to apparent relative molal enthalpies based on Eq. (30)

$$\Delta_{sol}H_m(m) = \Delta_{sol}H_m(\infty) + {}^{\phi}L_m(m) \tag{30}$$

where $\Delta_{sol}H_m(m)$, $\Delta_{sol}H_m(\infty)$ and ${}^{\phi}L_m(m)$ are the integral heat of solution at concentration m, the integral heat of solution at infinite dilution, and the apparent relative molal enthalpy at concentration m, respectively.

Specific heat capacity data are converted to apparent molal heat capacity of solute with Eq. (31)

$${}^{\phi}C_{p,m}(m) = M_s c_p(m) + \frac{1000}{m}(c_p(m) - c_p^0) \tag{31}$$

where ${}^{\phi}C_{p,m}(m)$ is the apparent molal heat capacity of solute, $c_p(m)$ and $c_p{}^0$ are the specific heat of aqueous solution concentration m and the specific heat of pure water, respectively. M_s is the molar mass of the solute.

Table 4
Literature data on the temperature and the saturated solution composition at two-solid saturation points of the LiCl+H_2O system.

Solid phases	Trans. Temp. (K)	Comp. (wt%)	Ref.
Eutectic point Ice+LiCl · $5H_2O$	189.15	25.2	[62]
	193.15	25.3	[98]
	198.15	24.8	[99]
	197.25	25.02	[100]
	197.65	25.3	[101]
	194.95	25.33	[102]
	193.88	25.64	[103]
	194.9	25.76	This work
Peritectic point LiCl · $5H_2O$+LiCl · $3H_2O$	205.95	29.3	[62]
	207.75	29.15	[81]
	205.15	28.7	[98]
	208.65	31.2	[99]
	207.75	29.39	[100]
	204.95	28.7	[101]
	205.95	29.05	[102]
	205.02	28.74	[103]
	206.35	29.0	This work
Peritectic point LiCl · $3H_2O$+LiCl · $2H_2O$	254.15	38.0	[62]
	252.65	37.8	[81]
	253.15	36.9	[98]
	255.15	38.5	[99]
	255.89	38.23	[100]
	253.25	36.9	[101]
	253.65	37.59	[102]
	254.18	37.46	[103]
	253.25	37.8	This work
Peritectic point LiCl · $2H_2O$+LiCl · H_2O	292.25	45.2	[62]
	292.55	45.15	[81]
	285.65	40.5	[98]
	291.65	45	[99]
	293.94	45.34	[100]
	292.25	45.2	[101]
	293.05	45.32	[102]
	293.86	45.54	[103]
	292.4	45.23	This work
Peritectic point LiCl · H_2O+LiCl	366.65	–	[67]
	373.65	56.5	[98]
	371.15	56.7	[99]
	369.74	56.19	[100]
	366.95	55.8	[101]
	369	56.30	[102]
	367.15	–	[104]
	366.65	55.74	This work

4. Thermodynamic modeling of the LiCl+H_2O system

To determine the model parameters of the LiCl+H_2O system, the water activity (or osmotic coefficient), the mean ionic activity coefficients, the enthalpy of dilution and solution, the heat capacity of the aqueous phase and solubility data are used. The data used are listed in Table 1, and cover a temperature range from 194 K to 443 K and a concentration range from infinitely dilute to the solubility limit.

The temperature coefficients *A*, *B*, *C*, *D* and *E* in the heat capacity, standard Gibbs energy, enthalpy and entropy equations of LiCl (cr) are taken from the NIST Webbook directly. Eq. (25) is used to represent the temperature dependence of the heat capacity for LiCl · H_2O(cr), LiCl · $2H_2O$(cr), LiCl · $3H_2O$(cr) and LiCl · $5H_2O$(cr). The remaining coefficients *F* and *G* for LiCl(cr) and *B*, *F* and *G* for LiCl · H_2O(cr), LiCl · $2H_2O$(cr), LiCl · $3H_2O$(cr) and LiCl · $5H_2O$(cr) are determined together with the PSC equation parameters in one simultaneous regression. The obtained standard Gibbs energy equations for all of the species are shown in Table 2.

The regressed PSC equation parameters for LiCl(aq) are listed in Table 3 with the temperature dependence of Eq. (8). The standard deviations of the overall fitting with respect to the terms ln a_w, ln $\gamma_{\pm}$, $\Delta_{dil}H_m/RT$, ${}^{\phi}L_m/RT$, ${}^{\phi}C_{p,m}/R$, and ln *K* are 0.007, 0.085, 0.0324, 0.0218, 0.1358, 0.3207, and 0.0286, respectively.

4.1. Water activity

The standard deviations of the water activity at all temperatures are 0.0024 and 0.01 for the unsaturated and saturated solutions, respectively. The water activity deviations between the literature and the values computed in this work for the unsaturated solutions are shown in Fig. 1. Most derivations fall in the range of $\pm$0.005. At 298.15 K, our model values agreed with the recommended values [45,51].

The data (crossed star in Fig. 1) of Pearce and Nelson [56] at 298.15 K depart from the model values significantly with a maximum error of 0.0135; thus, they are unreliable. The same conclusion has been drawn by Zeng and Zhou [91].

The deviations of the model values from the experimental data (open down-triangle in Fig. 1) reported by Holmes and Mesmer [46] are relatively large. Possibly, the validity of the model decreases at high temperatures.

4.2. Mean ionic activity coefficient

In the parameter regression, the literature data [45,51,69,70] for the mean ionic activity coefficients of LiCl(aq) are applied. Among them, the data from [69,70] are electrochemical cell results, and the data from [45,51] are recommended. The model values in this work agree with the data [45,51,70] satisfactorily, as shown in Fig. 2. The experimental data reported by Caramazza [70] are remarkably scattered. It is pleasing that the model results in this work agree with another set of model values reported by Gibbard and Scatchard [44] over a wide temperature range, as shown in Fig. 3, although the latter are never used in the parameter regression.

In our previous work [92], the PSC model parameters were determined by fitting to the water activities only. However, the calculated salt activity coefficients with these parameters differ from the present work remarkably, as shown in Fig. 4. The present model parameters are more reasonable, as they were obtained under more thermodynamic constraints.

4.3. Thermal properties of LiCl(aq)

The standard deviation of the overall fitting for the enthalpy of dilution, enthalpy of solution, and apparent molal heat capacity are 67 J mol^{-1}, 300 J mol^{-1}, and 2.7 J K^{-1} mol^{-1}, respectively.

The enthalpy of dilution of LiCl(aq) calculated in this work agrees with the experimental data [71, 76] very well at 298.15 K and 373.15 K, however, quite differ from the values calculated by the Pitzer model parameters given by Holmes and Mesmer [93] at 298.15 K, as shown in Figs. 5 and 6. We notice that Holmes and Mesmer [93] evaluated their Pitzer model parameters in the LiCl concentrations below 9.443 mol kg^{-1}. At higher LiCl concentrations, the validity of the model parameters could be weak.

Fig. 7 showed that the apparent relative molal enthalpy of LiCl (aq) calculated in this work agrees with those reported by Gibbard and Scatchard [44] very well, although the latter is not used in the present parameter regression.

Equivalently to the enthalpy of dilution, the apparent relative molal enthalpies of LiCl(aq) in this work differ from the model

Table 5
Standard state thermodynamic values of solid phases at 298.15 K in LiCl+H_2O system.

Solids	$\Delta_f G^0_m$ (kJ mol^{-1})	$\Delta_f H^0_m$ (kJ mol^{-1})	S^0_m (J mol^{-1} K^{-1})	$C^0_{p,m}$ (J mol^{-1} K^{-1})	Ref.
LiCl(cr)	−389.72	−414.8	56.5	234.0	[100]
	−384.015	−408.26	–	48.03	[103]
	−384.37	−408.61	59.33	47.99	[105]
	−385.531	–	52.206	48.037	[106]
	−385.07	−408.85	59.06	48.04	This work
LiCl · H_2O(cr)	−632.02	−714.55	97.18	494.1	[100]
	−631.8	−698.499	–	89.063	[103]
	−631.8	−712.58	102.84	–	[105]
	−631.728	–	101.838	84.4456	[106]
	−631.22	−712.91	99.87	91.53	This work
LiCl · 2H_2O(cr)	−869.14	−1013.7	139.2	–	[100]
	−874.244	−996.125	–	130.095	[103]
	–	−1012.65	–	–	[105]
	−874.136	–	145.901	130.001	[106]
	−873.51	−1013.32	138.22	135.03	This work
LiCl · 3H_2O(cr)	−1106.27	−1309.12	188.3	–	[100]
	−1114.98	−1287.94	–	171.128	[103]
	–	−1311.3	–	–	[105]
	−1114.73	–	198.775	113.456	[106]
	−1112.50	−1315.86	158.31	178.53	This work
LiCl · 5H_2O(cr)	−1580.53	−1889.11	302.24	–	[100]
	−1592.2	−1871.19	–	253.193	[103]
	−1592.53	–	337.3417	298.807	[106]
	−1583.80	−1921.15	175.39	265.53	This work

values by Holmes and Mesmer [93], as seen in Fig. 8.

The differences of the apparent molal heat capacity of LiCl(aq) between literature values and the model values in this work are plotted in Fig. 9. Most of the deviations falls in the range of ± 2.0 J K^{-1} mol^{-1}. The deviations increase reasonably at dilute solutions. Fig. 10 showed the calculated apparent molal heat capacity isotherms in this work compared with the experimental data from literature at 298.15 K, 323.15 K and 343.15 K. We can see the model reproduces these experimental data excellently.

4.4. Phase diagram, invariant points and saturated vapor pressures

Figs. 11 and 12 show the phase diagram of the LiCl+H_2O system and vapor pressures over saturated LiCl(aq) solutions, respectively. The calculated liquidus in the LiCl+H_2O system showed excellent agreement with the experimental results. Simultaneously, the predicted water vapor pressure of saturated LiCl(aq) solutions agrees with most literature data [66,67,94–96], though it does deviate from some literature data [68,97] in a certain temperature range. Notably, Greenspan [97] and Morillon et al. [68] reported the vapor pressure data without the corresponding solid phases. When we extrapolated the vapor pressure lines of LiCl · 2H_2O and LiCl · H_2O to the lower meta-stable temperature ranges, the calculated results agree with the literature data [68,97] very well. Possibly, the authors reported the vapor pressure data at meta-stable states.

Invariant points in the LiCl+H_2O system predicted from this model are listed in Table 4 and compared with literature values. The predicted invariant points agree with the most recent evaluations of Pátek and Klomfar [102] very well, except for the peritectic point for LiCl · H_2O+LiCl.

4.5. Standard state thermodynamics of the solid phases

The determined thermodynamic values of the solid phases at the standard state and 298.15 K are listed in Table 5. The thermodynamic values ($\Delta_f G^0_m$, $\Delta_f H^0_m$, S^0_m, $C^0_{p,m}$) for LiCl(cr), LiC · H_2O(cr) and LiCl · 2H_2O(cr) produced in this work agree with the literature values [100, 103, 105, 106] very well, except for the heat capacity values of LiCl(cr) and LiCl · H_2O(cr) given by Monnin et al.[100]. These heat capacities of solids are significantly larger than the values from others. Slight differences appear in the data for the solids LiCl · 3H_2O(cr). Obvious inconsistency of the data for the solid phase LiCl · 5H_2O(cr) at 298.15 K arise among all of the reported data, including the present work. After all, extrapolation of data from the deeply low temperatures (195–206 K) to 298 K is a challenge for all researchers when the heat capacities of supercooled liquid water are unknown at such low temperatures. Fortunately, the thermodynamic data of LiCl · 3H_2O(cr) and LiCl · 5H_2O(cr) are more important at lower temperatures than at 298 K, as these phases can only exist in multi-component systems at temperatures lower than their stable formation temperatures in binary systems based on the phase diagram rule.

5. Conclusions

The PSC model is selected to represent the thermodynamic properties of the salt lake brine systems containing Li-salts at multiple temperatures. The temperature dependence of the thermodynamic functions (entropy, enthalpy and Gibbs energy) for the aqueous species and the solid phases are determined using their heat capacities. In this way, the thermodynamic inner consistence of the parameters is held. Comprehensive thermodynamic properties, i.e., water activity, mean ionic activity coefficient, enthalpy of dilution and solution, heat capacity and solubility, are used to evaluate the model parameters. The proposed parameter regression strategy has proven successful in the highly soluble LiCl+H_2O system, and the present thermodynamic model of the LiCl+H_2O system is valid in the temperature range of 190 K to nearly 400 K. The present work forms a solid foundation for the thermochemical properties simulation of other complicated salt lake brine systems.

Acknowledgments

This work was financially supported by KLSLRC (Grant 221 KLSLRC-KF-13-HX-3) and the National Natural Science Foundation of China (U1407131).

Appendix A. Supplementary material

Supplementary data associated with this article can be found in the online version at http://dx.doi.org/10.1016/j.calphad.2015.05.001.

References

[1] P.S. Song, Y. Yao, Thermodynamics and phase diagram of the salt lake brine system at 298.15 K: V. Model for the system Li^+, Na+, K^+, Mg^{2+}/Cl^-, SO_4^{2-}–H_2O and its applications, CALPHAD 27 (2003) 343–352.
[2] K.S. Pitzer, Activity Coefficients in Electrolyte Solutions, 2nd edition,. CRC Press, Boca Raton, 1991.
[3] P.S. Song, Y. Yao, Parameters of Pitzer model for the salt lake brine system and their applications I. Applications in physical chemistry for the system Li^+, Na^+, K^+, Mg^{2+}/Cl^-, SO_4^{2-}–H_2O, J. Salt Lake Res. 11 (3) (2003) 1–7.
[4] P.S. Song, Y. Yao, Parameters of Pitzer model for the salt lake brine system and their applications II. Prediction of solubilities in the system Li^+, Na^+, K^+, Mg^{2+}/Cl^-, SO_4^{2-}–H_2O, J. Salt Lake Res. 11 (4) (2003) 1–11.
[5] P.S. Song, Y. Yao, Parameters of Pitzer model for the salt lake brine system and their applications III. Applications in process technology in the system Li^+, Na^+, K^+, Mg^{2+}/Cl^-, SO_4^{2-}–H_2O, J. Salt Lake Res. 12 (3) (2004) 1–10.
[6] K.S. Kwok, K.M. Ng, M.E. Taboada, L.A. Cisternas, Thermodynamics of salt lake system: representation, experiments, and visualization, AIChE J. 54 (2008) 706–727.
[7] K. Thomsen, Aqueous electrolytes: model parameters and process simulation (Doctoral dissertation), 1997.
[8] Z. Nie, L. Bu, M.P. Zheng, W. Huang, Experimental study of natural brine solar ponds in Tibet, Sol. Energy 85 (2011) 1537–1542.
[9] C.E. Harvie, J.H. Weare, The prediction of mineral solubilities in natural waters: the Na–K–Mg–Ca–Cl–SO_4–H_2O system from zero to high concentration at 25 °C, Geochim. Cosmochim. Acta 44 (1980) 981–997.
[10] C.E. Harvie, N.M. Moller, J.H. Weare, The prediction of mineral solubilities in natural waters: the Na–K–Mg–Ca–H–Cl–SO_4–H–HCO_3–CO_3–CO_2–H_2O system to high ionic strengths at 25 °C, Geochim. Cosmochim. Acta 48 (1984) 723–752.
[11] N. Moller, The prediction of mineral solubilities in natural waters: a chemical equilibrium model for the Na–Ca–Cl–SO_4–H_2O system, to high temperature and concentration, Geochim. Cosmochim. Acta 52 (1988) 821–837.
[12] J.P. Greenberg, N. Moller, The prediction of mineral solubilities in natural waters: a chemical equilibrium model for the Na–K–Ca–Cl–SO_4–H_2O system to high concentration from 0 to 250 °C, Geochim. Cosmochim. Acta 53 (1989) 2503–2518.
[13] R.J. Spencer, N. Moller, J.H. Weare, The prediction of mineral solubilities in natural water: a chemical equilibrium model for the Na–K–Ca–Mg–Cl–SO_4–H_2O system at temperature below 25 °C, Geochim. Cosmochim. Acta 54 (1990) 575–590.
[14] G.M. Marion, R.E. Farren, Mineral solubilities in the Na–K–Mg–Ca–Cl–SO_4–H_2O system: a re-evaluation of the sulfate chemistry in the Spencer–Moller–Weare model, Geochim. Cosmochim. Acta 63 (1999) 1305–1318.
[15] X. Yin, Q.X. Li, Y.P. Wan, B.H. Li, D.W. Zeng, Comparison of thermodynamic models in high-solubility salt+H_2O systems I: binary systems, Acta Chim. Sin. 66 (2008) 1815–1826.
[16] H.T. Kim, W.J. Frederick Jr., Evaluation of Pitzer ion interaction parameters of aqueous electrolyte at 25 °C. 1. Single salt parameters, J. Chem. Eng. Data 33 (1988) 177–184.
[17] H.F. Holmes, R.E. Mesmer, Thermodynamic properties of aqueous solutions of the alkali metal chlorides to 250 °C, J. Phys. Chem. 87 (1983) 1242–1255.
[18] H.F. Holmes, R.H. Busey, J.M. Simonson, R.E. Mesmer, $CaCl_2$(aq) at elevated temperatures. enthalpies of dilution, isopiestic molalities, and thermodynamic properties, J. Chem. Thermodyn. 26 (1994) 271–298.
[19] H.F. Holmes, R.E. Mesmer, Aqueous solutions of the alkaline-earth metal chlorides at elevated temperatures. Isopiestic molalities and thermodynamic properties, J. Chem. Thermodyn. 28 (1996) 1325–1358.
[20] K.S. Pitzer, J.M. Simonson, Thermodynamics of multi-component, miscible, ionic systems: theory and equations, J. Phys. Chem. 90 (1986) 3005–3009.
[21] J.M. Simonson, K.S. Pitzer, Thermodynamics of multi-component, miscible, ionic systems: the system $LiNO_3$–KNO_3–H_2O, J. Phys. Chem. 90 (1986) 3009–3013.
[22] S.L. Clegg, K.S. Pitzer, Thermodynamics of multi-component, miscible, ionic solutions: generalized equations for symmetrical electrolytes, J. Phys. Chem. 96 (1992) 3513–3520.
[23] S.L. Clegg, K.S. Pitzer, P. Brimblecombe, Thermodynamics of multi-component, miscible, ionic solutions. 2. Mixtures including unsymmetrical electrolytes, J. Phys. Chem. 96 (1992) 9470–9479.
[24] S.L. Clegg, S.S. Ho, C.K. Chan, P. Brimblecombe, Thermodynamic properties of aqueous $(NH_4)_2SO_4$ to high supersaturation as a function of temperature, J. Chem. Eng. Data 40 (1995) 1079–1090.
[25] S.L. Clegg, P. Brimblecombe, A.S. Wexler, Thermodynamic model of the system H^+–NH_4^+–Na^+–SO_4^{2-}–NO_3^-–Cl^-–H_2O at 298.15 K, J. Phys. Chem. A 102 (1998) 2155–2171.
[26] E. Friese, A. Ebel, Temperature dependent thermodynamic model of the system H^+–NH_4^+–Na^+–SO_4^{2-}–NO_3^-–Cl^-–H_2O, J. Phys. Chem. A 114 (2010) 11595–11631.
[27] D.J. Bradley, K.S. Pitzer, Thermodynamics of electrolytes. 12. Dielectric properties of water and Debye–Hückel parameters to 350 °C and 1 kbar, J. Phys. Chem. 83 (1979) 1599–1603.
[28] W. Wagner, A. Pruss, International equations for the saturation properties of ordinary water substance. revised according to the international temperature scale of 1990. Addendum to J. Phys. Chem. Ref. Data 16, 893 (1987), J. Phys. Chem. Ref. Data 22 (1993) 783–787.
[29] H.Y. Afeefy, J.F. Liebman, S.E. Stein, in: P.J. Linstrom, W.G. Mallard (Eds.), "Neutral Thermochemical Data" in NIST Chemistry WebBook, NIST Standard Reference Database Number 69, National Institute of Standards and Technology, Gaithersburg MD, 2014, p. 20899 (retrieved 23.7.2014).
[30] H.C. Helgeson, D.H. Kirkham, G.C. Flowers, Theoretical prediction of the thermodynamic behavior of aqueous electrolytes at high pressure and temperatures: IV. Calculation of activity coefficients, osmotic coefficients, and apparent molal and standard and relative partial molal properties to 600 °C and 5 kbar, Am. J. Sci. 28 (1981) 1249–1516.
[31] E.L. Shock, H.C. Helgeson, Calculation of thermodynamic and transport properties of aqueous species at high pressures and temperatures: correlation algorithms for ionic species and equation of state predictions to 5 kbar and 1000 °C,, Geochim. Cosmochim. Acta 52 (1988) 2009–2036.
[32] J.M. Dick, Calculation of the relative metastabilities of proteins using the CHNOSZ software package, Geochem. Trans. 9 (2008) 1–17.
[33] S.L. Clegg, P. Brimblecombe, Application of a multi-component thermodynamic model to activities and thermal properties of 0 – 40 mol kg^{-1} aqueous sulfuric acid from < 200 to 328 K, J. Chem. Eng. Data 40 (1995) 43–64.
[34] C.A. Angell, M. Ogunl, W.J. Slchlna, Heat capacity of water at extremes of supercooling and superheating, J. Phys. Chem. 86 (1982) 998–1002.
[35] D.G. Archer, R.W. Carter, Thermodynamic properties of the NaCl+H_2O system. 4. Heat capacities of H_2O and NaCl(aq) in cold-stable and supercooled states, J. Phys. Chem. B 104 (2000) 8563–8584.
[36] R. Feistel, W. Wagner, A New equation of state for H_2O ice Ih, J. Phys. Chem. Ref. Data 35 (2006) 1021–1047.
[37] P.M. Kobylin, H. Sippola, P.A. Taskinen, Thermodynamic modelling of aqueous Fe(II) sulfate solutions, CALPHAD 35 (2011) 499–511.
[38] D.G. Archer, Thermodynamic properties of the NaCl+H_2O system II. Thermodynamic properties of NaCl(aq), NaCl•$2H_2O$(cr), and phase equilibria, J. Phys. Chem. Ref. Data 21 (1992) 793–829.
[39] M. Galassi, J. Davies, J. Theiler, B. Gough, G. Jungman, P. Alken, M. Booth, F. Rossi, GNU Scientific Library, Reference Manual, Edition 1.1.5, for GSL Version 1.15, 29 Apr. 2011.
[40] K.S. Pitzer, J.C. Pelper, R.H. Busey, Thermodynamic properties of aqueous sodium chloride solutions, J. Phys. Chem. Ref. Data 13 (1984) 1–102.
[41] P.G. Hill, A unified fundamental equation for the thermodynamic properties of H_2O, J. Phys. Chem. Ref. Data 19 (1990) 1233–1274.
[42] T.M. Davis, L.M. Duckett, J.F. Owen, C.S. Patterson, R. Saleeby, Osmotic coefficients of aqueous LiCl and KCl from their isopiestic ratios to NaCl at 45 °C, J. Chem. Eng. Data 30 (1985) 432–434.
[43] T.M. Davis, L.M. Duckett, C.E. Garvey, J.M. Hollfield, C.S. Patterson, Osmotic coefficients of aqueous LiCl and $CaCl_2$ from their isopiestic ratios to NaCl at 50 °C, J. Chem. Eng. Data 30 (1985) 432–434.
[44] H.F. Gibbard Jr., G. Scatchard, Liquid-vapor equilibrium of aqueous lithium chloride, from 25 °C to 100 °C and from 1.0 to 18.5 molal, and related properties, J. Chem. Eng. Data 18 (1973) 293–298.
[45] W.J. Hamer, Y.C. Wu, Osmotic coefficients and mean activity coefficients of uni-univalent electrolytes in water at 25 °C, J. Phys. Chem. Ref. Data 1 (1972) 1047–1100.
[46] H.F. Holmes, R.E. Mesmer, Isopiestic studies of aqueous solutions at elevated temperature VI. LiCl and CsCl, J. Chem. Thermodyn. 13 (1981) 1035–1046.
[47] W. Kangro, A. Groeneveld, Konzentrierte wäßrige Lösungen, I, Zeitschrift für, Phys. Chem. Neue Folge 32 (1962) 110–126.
[48] W.T. Lindsay, C.T. Liu, , Osmotic coefficients of one molal alkali metal chloride solutions, J. Phys. Chem. 75 (1971) 3723–3727.
[49] L.J. Guo, B. Sun, D.W. Zeng, Y. Yao, H.J. Han, Isopiestic measurement and solubility evaluation of the ternary system LiCl–$SrCl_2$–H_2O at 298.15 K, J. Chem. Eng. Data 57 (2012) 817–827.
[50] Y. Yao, B. Sun, P.S. Song, Z. Zhang, Thermodynamics of aqueous solution, isopiestic determination of osmotic and activity coefficients in LiCl–$MgCl_2$–H_2O at 25 °C, Acta Chim. Sin. 50 (1992) 839–848.
[51] R.A. Robinson, The water activities of lithium chloride solutions up to high concentration at 25 °C,, Trans. Farad. Soc. 41 (1945) 756–758.
[52] F.F. Li, Y. Yao, Isopiestic studies of thermodynamic properties in LiCl–Li_2SO_4–H_2O system at 273.15 K, Chem. Res. Appl. 16 (2004) 33–36.
[53] F.F. Li, Y. Yao, Isopiestic studies of thermodynamic properties of LiCl–Li_2SO_4–H_2O system at 323.15 K, J. Salt Lake Res. 12 (2004) 37–42.
[54] V. Brendler, W. Voigt, Isopiestic measurements at high temperatures: I. Aqueous solutions of LiCl, CsCl, and $CaCl_2$ at 155 °C, J. Solut. Chem. 23 (1994) 1061–1072.

[55] A. Lannung, Measurement of the vapor pressure of aqueous solutions of alkali halogenides,, Z. Phys. Chem. Abt. A 170 (1934) 134–144.
[56] J.N. Pearce, A.F. Nelson, The vapor pressures of aqueous solutions of lithium nitrate and the activity coefficients of some alkali salts in solutions to high concentration at 25 °C, J. Am. Chem. Soc. 54 (1932) 3544–3555.
[57] S.K. Chaudhari, K.R. Patil, Thermodynamic properties of aqueous solutions of lithium chloride, Phys. Chem. Liq. 40 (2002) 317–325.
[58] A.N. Campbell, O.N. Bhatnager, Osmotic and activity coefficients of lithium chloride in water from 50 to 150 °C, Chem. Can. J. 57 (1979) 2542–2545.
[59] C.S. Patterson, L.O. Gilpatrick, B.A. Soldano, The osmotic behaviour of representative aqueous salt solutions at 100 °C, J. Chem. Soc. (1960) 2730–2734.
[60] K.R. Patil, A.D. Tripathi, G. Pathak, S.S. Katti, Thermodynamic properties of aqueous electrolyte solutions. 1. Vapor pressure of aqueous solution of LiCl, LiBr, and LiI, J. Chem. Eng. Data 35 (1990) 166–168.
[61] W. Steudemann, Die thermische Analyse der Systeme des Wassers mit den Lithiumhalogeniden (Dissertation), Universität Jena, 1927.
[62] F.A. Schimmel, Solubilities of lithium chloride and lithium thiocyanate at low temperatures, J. Chem. Eng. Data 5 (1960) 519–520.
[63] H.F. Gibbard Jr., A. Fawaz, , Freezing points and related properties of electrolyte solutions. II. Mixtures of lithium chloride and sodium chloride in water, J. Solut. Chem. 3 (1974) 745–755.
[64] H.C. Jones, F.H. Getman, The molecular-lowering of the freezing-point of water produced by concentrated solutions of certain electrolytes,, Z. Phys. Chem. 32 (1904) 244–286.
[65] F. Momicchioli, O. Devoto, G. Grandi, G. Cocco, Thermodynamic properties of concentrated solutions of strong electrolytes I. Activity coefficients of water from freezing-point depressions for alkali chlorides, Ber. Bunsenges. Phys. Chem. 74 (1970) 59–66.
[66] F.C. Kracek, International Critical Tables, McGraw-Hill, New York (1928), p. 368.
[67] M.P. Applebey, F.H. Crawford, K. Gordon, Vapor pressure of saturated solutions. Lithium chloride and lithium sulphate, J. Chem. Soc. (1934) 1665–1671.
[68] V. Morillon, F. Debeaufort, J. Jose, J.F. Tharrault, M. Capelle, G. Blond, A. Voilley, Fluid Phase Equilib. 155 (1999) 297–309.
[69] Y. Yao, R. Wang, X. Ma, P.S. Song, Thermodynamic properties of aqueous mixture of LiCl and Li_2SO_4 at different temperatures, J. Therm. Anal. 45 (1995) 117–130.
[70] R. Caramazza, Coefficienti di attività di elettroliti forti in soluzioni acquose concentrate—Nota I. Cloruro di litio, Ann. Chim 53 (1963) 472–480.
[71] J.E. Mayrath, R.H. Wood, Enthalpy of dilution of aqueous solutions of LiCl, NaBr, NaI, KCl, KBr, and CsCl at about 373, 423, and 473 K, J. Chem. Thermodyn. 14 (1982) 563–576.
[72] W.H. Leung, F.J. Millero, The enthalpy of formation of magnesium sulfate ion pairs, J. Solut. Chem. 4 (1975) 145–159.
[73] R.H. Wood, R.A. Rooney, J.N. Braddock, Heats of dilution of some alkali metal halides in deuterium oxide and water, J. Phys. Chem. 78 (1969) 1673–1678.
[74] T.W. Richards, A.W. Rowe, The heats of dilution and the specific heats of dilute solutions of nitric acid and of hydroxides and chlorides and nitrates of lithium, sodium, potassium, and cesium, J. Am. Chem. Soc. 43 (1921) 770–796.
[75] Y.C. Wu, T.F. Young, Enthalpies of dilution of aqueous electrolytes: sulfuric acid, hydrochloric acid, and lithium chloride, J. Res. Natl. Bur. Stand. 85 (1980) 11–17.
[76] E. Lange, F. Dürr, Lösungs- und verdünnungswarmen von salzen von grosser verdünnung bis zur sättigung. II. Lithiumchlorid, Z. Phys. Chem. 12 (1926) 361–384.
[77] J.L. Fortier, P.A. Leduc, J.E. Desnoyers, Thermodynamic properties of alkali halides. II. Enthalpies of dilution and heat capacities in water at 25 °C, J. Solut. Chem. 3 (1974) 323–349.
[78] H. Rüterjans, F. Schreiner, U. Sage, Th Ackermann, Apparent molal heat capacities of aqueous solutions of alkali halides and alkylammonium salt, J. Phys. Chem. 73 (1969) 986–994.
[79] F.T. Gucker, K.H. Schminke, A study of the heat capacity and related thermodynamic properties of aqueous solutions of lithium chloride, hydrochloric acid and potassium hydroxide at 25 °C, J. Am. Chem. Soc. 54 (1932) 1358–1373.
[80] Y. He, N. Gao, G. Chen, Isobaric specific heat capacity of typical lithium chloride liquid desiccants using scanning calorimetry, J. Chem. Thermodyn. 70 (2014) 81–87.
[81] J.J. Kessis, Syèteme eau-chlorure de lithium (suite). Mesures de solubilité entre −65 et +60 °C, Bull. Soc. Chim. Fr. (1961) 1503–1504.
[82] H. Benrath, Die polythermen der ternären systeme: $CuCl_2$–$(LiCl)_2$–H_2O und $NiCl_2$–$(LiCl)_2$–H_2O, Z. Anorg. Allg. Chem. 205 (1932) 417–424.
[83] H. Benrath, Die polytherme des ternären systeme: $MnCl_2$–$(LiCl)_2$–H2O, Z. Anorg. Allg. Chem. 220 (1934) 145–153.
[84] H. Benrath, Das System Kobaltchlorid—Lithiumchlorid—Wasser, Z. Anorg. Allg. Chem. 240 (1938) 87–96.
[85] H. Bassett, I. Sanderson, The compounds of lithium chloride with cobalt chloride. Water as a linking agent in polyunclear kations, J. Chem. Soc. (1932) 1855–1864.
[86] D.W. Zeng, J.W. Ming, W. Voigt, Thermodynamic study of the system ($LiCl+LiNO_3+H_2O$), J. Chem. Thermodyn. 40 (2008) 232–239.
[87] D.W. Zeng, W.F. Xu, W. Voigt, X. Yin, , Thermodynamic study of the system ($LiCl+CaCl_2+H_2O$), J. Chem. Thermodyn. 40 (2008) 1157–1165.
[88] J.A.N. Friend, A.T.W. Colley, The solubility of lithium chloride in water, J. Chem. Soc. (1931) 3148–3149.
[89] J.N. Friend, R.W. Hale, S.E.A. Ryder, The solubility of lithium chloride in water between 70 °C to 160 °C, J. Chem. Soc. (1937) 970.
[90] M.A. Clynne, R.W. Potter II, Solubility of some alkali and alkaline earth chlorides in water at moderate temperatures, J. Chem. Eng. Data 24 (1979) 338–340.
[91] D.W. Zeng, J. Zhou, Thermodynamic consistency of the solubility and vapor pressure of a binary saturated salt+water system. 1. $LiCl+H_2O$, J. Chem. Eng. Data 51 (2006) 315–321.
[92] H.T. Ouyang, D.W. Zeng, H.Y. Zhou, H.J. Han, Y. Yao, Solubility of the ternary system $LiCl+NH_4Cl+H_2O$, J. Chem. Eng. Data 56 (2011) 1096–1104.
[93] H.F. Holmes, R.E. Mesmer, Thermodynamic properties of aqueous solutions of the alkali metal chlorides to 250 °C, J. Phys. Chem. 87 (1983) 1242–1255.
[94] C.P. Hedlin, F.N. Trofimenkoff, Relative humidities over saturated solutions of nine salts in the temperature range from 0 to 90 °F,, in: A. Wexler, W. A. Wildhack (Eds.), Humidity and Moisture—Fundamentals and Standards, vol. 3, Reinhold, New York, 1965, pp. 519–520.
[95] D.T. Acheson, Vapor pressures of saturated aqueous salt solutions, in: A. Wexler, W.A. Wildhack (Eds.), Humidity and Moisture—Fundamentals and Standards, vol. 3, Reinhold, New York, 1965, p. 521.
[96] C. Arai, S. Hosaka, K. Murase, Y. Sano, Measurements of the relative humidity of saturated aqueous salt solutions, J. Chem. Eng. Jpn. 9 (1976) 328–330.
[97] L. Greenspan, Humidity fixed points of binary saturated aqueous solutions, J. Res. Natl. Bur. Stand. 81A (1977) 89–96.
[98] G.H. Hüttig, W. Steudemann, Studien zur Chemie des Lithiums. VI. Die thermische Analyse der Systeme Lithiumhalogenide-Wasser, Z. Phys. Chem. 126 (1927) 105–117.
[99] E.A. Akopov, Polytherm solubility of LiCl–KCl–H_2O system, Zh. Neorg. Khim. 7 (1962) 385–388.
[100] C. Monnin, M. Dubois, N. Papaiconomou, J.P. Simonin, Thermodynamics of $LiCl+H_2O$ system, J. Chem. Eng. Data 47 (2002) 1331–1336.
[101] M.R. Conde, Properties of aqueous solutions of lithium and calcium chlorides: formulations for use in air conditioning equipment design, Int. J. Therm. Sci. 43 (2004) 367–382.
[102] J. Pátek, J. Klomfar, Solid–liquid phase equilibrium in the systems of LiBr–H_2O and LiCl–H_2O, Fluid Phase Equilib. 250 (2006) 138–149.
[103] M.Y. Li, L.S. Wang, J. Gmehling, Thermodynamics of phase equilibria in aqueous strong electrolyte systems, Ind. Eng. Chem. Res. 50 (2011) 3621–3631.
[104] H.E. Moran, System lithium chloride–water, J. Phys. Chem. 60 (1956) 1666–1667.
[105] D.D. Wagman, W.H. Evans, V.B. Parker, R.H. Schumm, I. Halow, S.M. Bailey, K. L. Churney, R.L. Nuttall, The NBS tables of chemical thermodynamic properties. Selected values for inorganic and C_1 and C_2 organic substances in SI units, J. Phys. Chem. Ref. Data 11 (1982) 1–392.
[106] M.S. Gruszkiewicz, D.A. Palmer, R.D. Springer, P. Wang, A. Anderko, Phase behavior of aqueous Na–K–Mg–Ca–Cl–NO_3 mixtures: isopiestic measurements and thermodynamic modeling, J. Solut. Chem. 36 (2007) 723–765.